P1.18 OBSERVATIONS AND STOCHASTIC MODELING OF SHORTWAVE RADIATIVE TRANSFER AT THE ARM CART SITES

Dana E. Lane-Veron* and Jaclyn M. Secora
Dept. of Environmental Sciences, Rutgers University

1. INTRODUCTION

Stochastic radiative transfer modeling is a promising approach to modeling the domain-averaged shortwave radiation fields that occur during scattered cloud conditions. A parameterization of the stochastic approach to modeling cloud-radiation interactions is being developed using archived data from the Atmospheric Radiation Measurement (ARM) Program's Clouds and Radiation Testbed (CART) sites. One year of continuously sampled data from all three CART sites (Southern Great Plains, Tropical Western Pacific, and North Slopes of Alaska) has been analyzed for input into the stochastic radiative transfer model, and a standard plane-parallel shortwave radiation model. Information about the cloud field characteristics such as cloud height, thickness, fraction and optical properties from 2000 are presented here for all three sites and compared to similar studies where appropriate (e.g. Lazarus et al. 2000). The output domain-averaged, shortwave radiation fields from the stochastic model will be evaluated using both observations and parallel plane model results.

2. DATA

In an earlier study, a novel method for investigating cloud spatial and physical properties using ground-based observations is presented (Lane et al. 2002). This preliminary research focused on low-level scattered clouds. For the work presented here, continuously sampled data from the Atmospheric Radiation Measurement Program (Stokes and Schwartz, 1994) are used to study the physical and geometric characteristics of the cloud fields over all three research sites, the Southern Great Plains (SGP), Tropical Western Pacific (TWP) and North Slope of Alaska (NSA). To date, analysis for all three sites over a one-year time period has been completed. The characteristic cloud base height, cloud thickness, cloud fraction, cloud size, effective radius and optical depth have been analyzed and are presented here as monthly means. When possible, these spatial characteristics have been compared to other available measurements (now shown). The data analysis will focus on providing the stochastic model with information similar to that calculated in an Atmospheric General Circulation Model (AGCM).

2.1 *Cloud base height*

The base height for each cloudy layer present during 2000 is taken from one of two sets of observations. The Belfort Laser Ceilometer (BLC) has high spatial resolution, but the laser is attenuated fairly low in the atmosphere (~12 km). The BLC cloud base heights were averaged over a one-hour period for input into the stochastic model and, additionally, monthly means were taken. At the NSA and TWP sites a BLC is not available and so a Vaisala Ceilometer (VCEIL) is used. Cloud base height measurements may also be taken from the Micropulse Lidar (MPL) observations. The MPL has poorer height resolution, but it is able to observe much higher clouds such as cirrus. This does not cause much of a disparity between the two instruments at the SGP site, but at the TWP and NSA sites, the MPL tends to produce monthly mean cloud base heights that are about 4 km higher than the BLC (not shown).

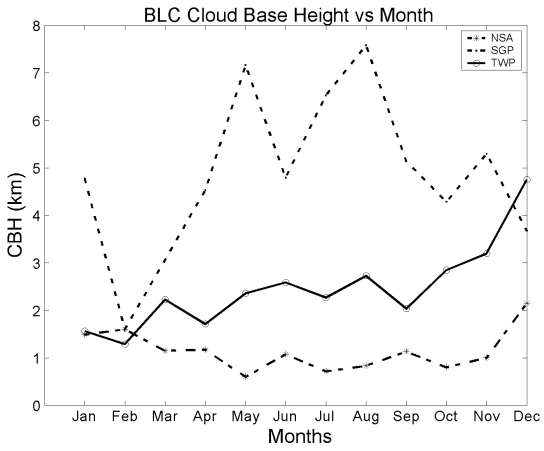

Figure 1. Monthly mean cloud base height as observed by the Belfort Laser Ceilometer or the Vaisala Ceilometer for the year 2000 at all three ARM CART Sites.

2.2 *Cloud Fraction*

The MPL is also used to determine a one-dimensional fraction by calculating the percentage of time that a cloud was detected relative to the entire time sampled. Hourly averages have again been compiled for all three sites, and Figure 2 shows the monthly mean cloud fractions. The NSA site tends to be overcast from May to November, with a cloud fraction below 80% during the rest of the year. The SGP site tends to have a cloud fraction of 60% to 80% all year. The TWP site shows cloud fractions between 70 and 80% all year, except during February and September, when the cloud fractions are around 65%. At the SGP site, in the first three months of 2000, the average cloud fraction was 0.64. January and March

* *Corresponding author address*: Dana E. Veron, veron@envsci.rutgers.edu; (732) 932-9081.

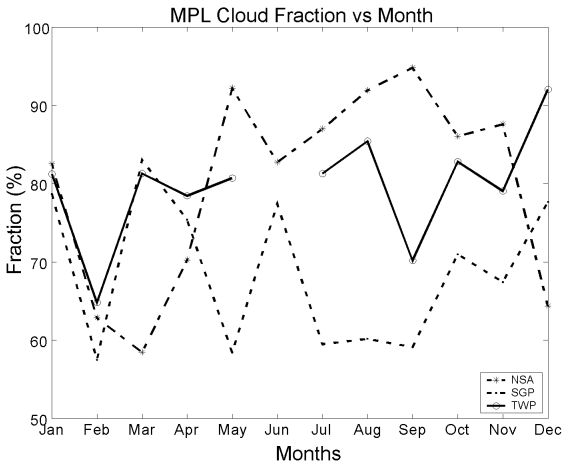

Figure 2. Monthly mean cloud fraction as observed by the Micropulse Lidar for the year 2000 at all three ARM CART Sites.

were cloudy about 75% of the time while in February clear sky was present 66% of the time.

In a previous study, several instruments, including the BLC, the Micropulse Lidar, Multifilter Rotating Shadowband Radiometer (MFRSR), and human observer reports of cloud fraction were compared. In all cases, the cloud fraction determined from measurements was less than the estimated cloud fraction from the observer. This difference in overhead and all-sky fraction has been reported by Bretherton et al. (1995).

2.3 *Cloud Chord Length*

The wind speed observed by the RWP915 is combined with cloud base height information from the VCEIL to give an indication of the size of overhead clouds. The MPL is used to calculate how long the direct normal beam is blocked by a cloud. A threshold is chosen to identify cloudy segments of the signal. Multiplying the time the sun was obscured by the wind speed at the base height of the cloud yields information about the cloud size. The lidar beam can be thought of as tracing a path from the leading edge to the trailing edge of a cloud (Figure 3).

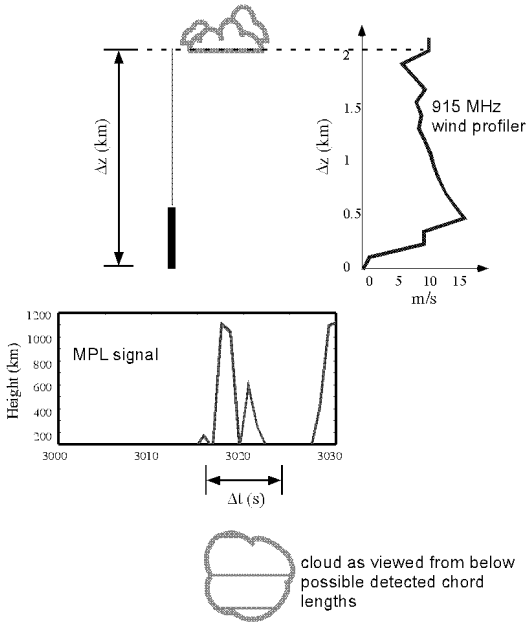

Figure 3. Illustration of the technique used to determine cloud horizontal scale using observed cloud base height and wind speed.

The resulting cloud chords are compiled in a probability frequency distribution. Previous results indicate that the statistics gathered at the Central Facility are well correlated (with a phase shift) over the rest of the facility. This result suggests that averaging a single station over long time-periods yield similar results to averaging over multiple horizontally distributed stations for shorter times. It is, therefore, possible to obtain robust statistics describing the cloud field from point measurements given enough time.

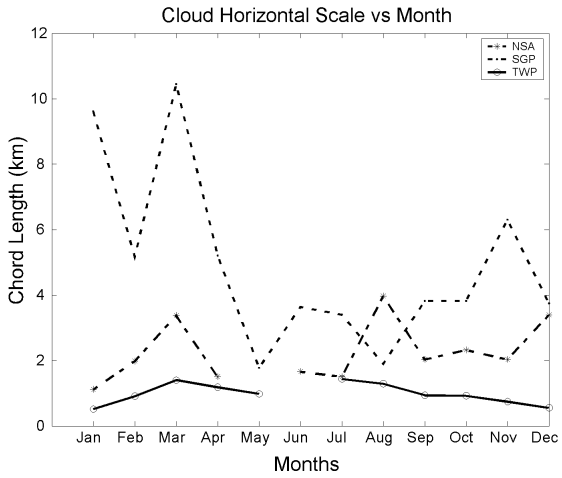

Figure 4. Monthly mean cloud horizontal scale (chord length) as determined from the Micropulse Lidar and RWP915 for the year 2000 at all three ARM CART Sites.

The monthly mean cloud chord length for all three sites is shown in Figure 4. The TWP and NSA sites tend to have smaller clouds, from 500 m to 4 km chord lengths. From January to April, the SGP site has very large chord lengths and then, during the rest of the year, they tend to be between 1 and 4km.

2.4 *Cloud Thickness*

The cloud thickness is calculated from the active remotely-sensed cloud locations (ARSCL) value added product (VAP) available in the ARM data archive. ARSCL combines data from laser ceilometers, microwave radiometers, and micropulse lidars to produce a time series of vertical distribution of cloud hydrometeors over the ARM sites. Two estimates of cloud base and top are provided, one using the Clothiaux et al. (2000) algorithm and the

other using Campbell et al. (1998) algorithm. The cloud thickness is determined by subtracting the cloud base height from the cloud top height.

Figure 5 shows the monthly mean cloud thickness for all three sites using the Clothiaux algorithm. Interestingly, the SGP and TWP sites have a similar variation in cloud thickness during the year. They each have a maximum thickness in May (~2.5 km) and a minimum in the late summer (~0.5 km). The NSA site shows a maximum thickness in the late summer (~2.3 km) and a minimum in March (~1 km).

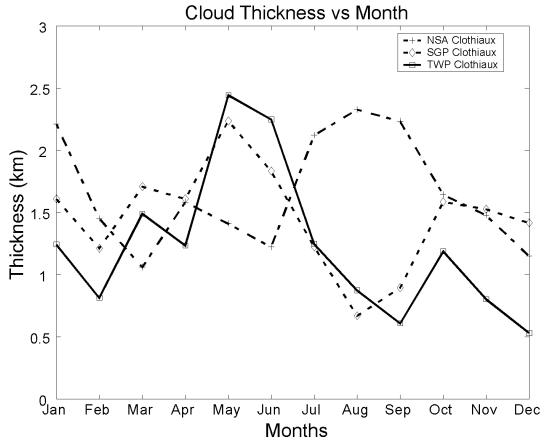

Figure 5. Monthly mean cloud thickness as determined from the ARSCL value added product for the year 2000 at all three ARM CART Sites.

2.5 *Droplet Radius/Optical Depth*

Cloud effective radius is computed using an algorithm developed by Dong et al., 1997. The top of figure 6 shows the monthly mean effective radius for the SGP site. There is a minimum in effective radius in August and September (~10 μm) and a maximum in March (75 μm). The minimum in May is due to a to a lack of data. The Dong et al. retrieval may only be used during daylight hours and when the sun angle is not too low.

The optical depth (τ) is computed using the equation: $\tau = 1.5 * LWP / r_{eff}$. The liquid water path observations are taken from the Microwave Radiometer and averaged on an hourly basis. The monthly mean optical depth for the SGP site is shown in the bottom of Figure 6. The SGP optical depths are variable, with a minimum in April of 3 and a maximum in July of 23.

3. MODELS

The observations described above are provided on an hourly basis to a stochastic shortwave radiative transfer model and a plane-parallel model. The resulting domain-averaged downwelling radiation is compared and evaluated against observations to determine the utility of the stochastic approach. Model runs are performed hourly for all three sites for all of 2000.

3.1 *Stochastic Model*

The stochastic model (Byrne et al. 1996) used in this study is comprised of a spectral radiative transfer model based on the exponential–sum fitting scheme of Wiscombe and Evans (1977). and a model atmosphere. There are 38 unequally spaced spectral bands, which range in wavenumber from 2500 cm^{-1} to 50000 cm^{-1}. Each band contains up to two absorbing gases, primarily water vapor and ozone, although carbon dioxide and molecular oxygen are also used.

The model is initialized with profiles of pressure, temperature, moisture, carbon dioxide and ozone taken from McClatchey's climatological values (McClatchey et al. 1972) for the appropriate season. The model atmosphere is divided into 32 layers, with a reflective surface. The model is applied to an area of approximately 250-km by 250-km, roughly equivalent to each of the CART sites (Lane-Veron and Somerville, 2004).

For this study, Markovian statistics for a mixture of cloud and clear sky are used. The distribution of each material is described by the chord lengths that are randomly selected from predetermined chord-length distributions – in this case distributions that were determined from observations as described in section 2.3. An example of this kind of distribution is shown in Figure 7. The cloudy material differs from clear sky in the liquid water content, and radiative properties. In general, the clouds occupy a fractional volume of the model layer. It is possible to have multiple layers of clouds, but there is no correlation in placement of the clouds between layers.

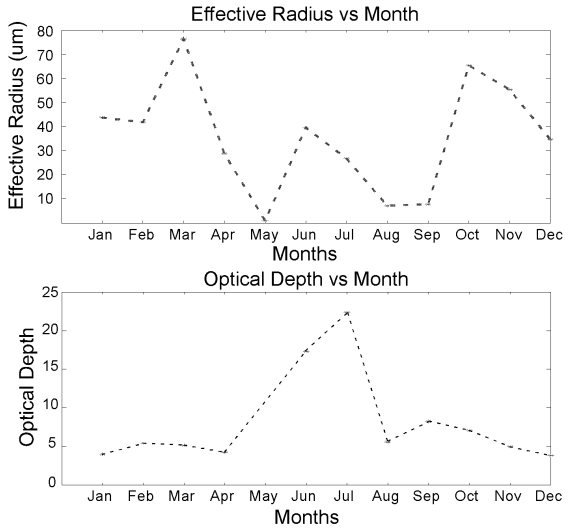

Figure 6. Top panel shows the monthly mean effective radius as derived using the Dong et al. (1997) retrieval at the SGP CART site for the year 2000. Bottom panel shows the optical depth for the same period.

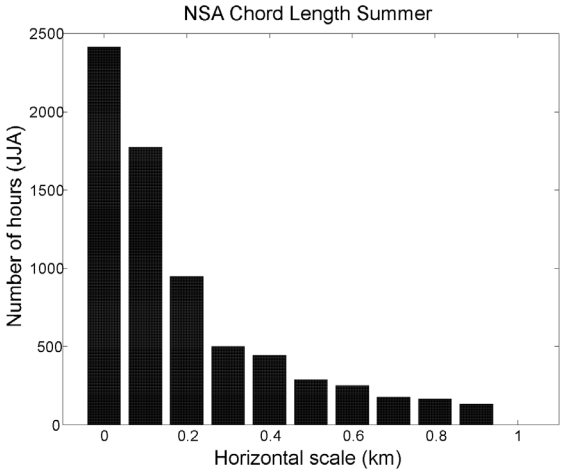

Figure 7. Example of histogram of cloud horizontal scale (chord length) for the NSA site for the summer of 2000.

The stochastic model is not appropriate for all cloudy situations. It is expected that the stochastic model will have the greatest influence when the cloud size is similar to the scale of a photon mean free path.

3.2 *Plane-parallel Model*

The Fouquart and Bonnel (1980) shortwave radiation routine, typical of those found in modern atmospheric general circulation models (AGCMs) is initialized using the same atmospheric profiles and run hourly using the same input data set (optical depth, cloud fraction) as the stochastic model. The plane-parallel model (SUNRAY) is not able to ingest information about the cloud horizontal scale. The model has 30 layers and two spectral bands.

3.3 *Results*

Figure 8 shows as comparison between the calculated downwelling shortwave radiation at the surface from stochastic model, the plane-parallel model and an observational network. Julian day 160 illustrates a situation where the stochastic model is more able to simulate the observed variability in the domain-averaged shortwave flux than the plane-parallel mode. The mean hourly cloud fraction is also shown in the same figure as early studies indicated that the performance of the stochastic model was related to the cloud fraction.

4. CONCLUSIONS

Stochastic shortwave radiative transfer theory is a promising approach for representing the influence of the macroscale cloud field structure on the domain-averaged radiation fields. Cloud field characteristics from the ARM CART sites may be used as appropriate input to the stochastic model. The resulting fluxes from the stochastic modeling technique are now being interpreted as a the basis of a new shortwave cloud-radiation parameterization for use in a AGCM.

Extension of the parameterization to one appropriate for a global model can be achieved in part by incorporating the North Slopes of Alaska and the Tropical Western Pacific CART sites. An important step in this process will be determination of when a stochastic cloud and radiation parameterization is appropriate, and how to identify these situations in an AGCM environment.

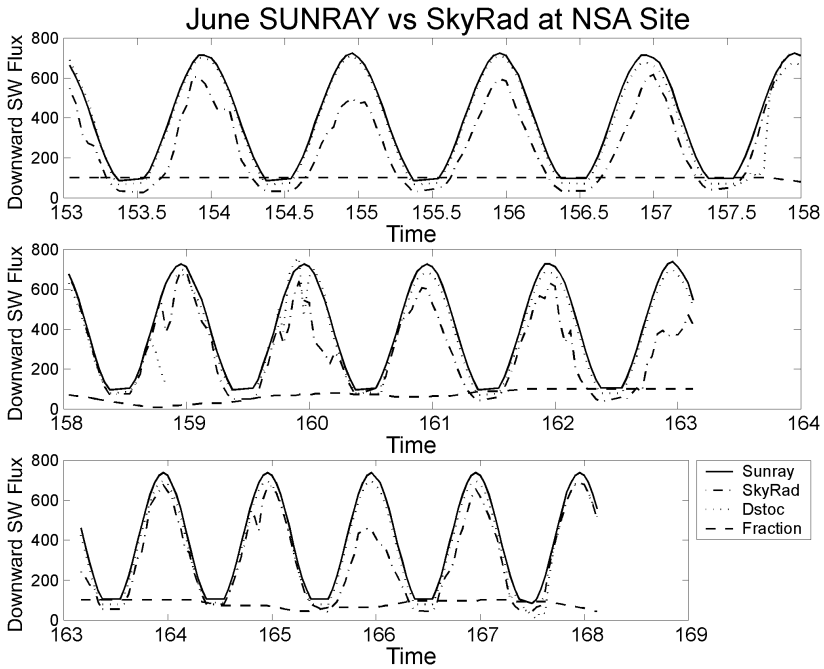

Figure 8. Comparison of modeled downwelling shortwave radiation from the stochastic model (DSTOC), the plane-parallel model (SUNRAY), observations (SkyRad), and overlaid with time-series of hourly cloud fraction for the NSA Site from June of 2000.

ACKNOWLEDGMENTS

This work was supported in part by the Department of Energy under Grant DOE DE-FG02-02ER63314.

REFERENCES

Bretherton, C. S., E. Klinker, A. K. Betts, and J. A. Coakley, Jr., 1995: Comparison of Ceilometer, Satellite and Synoptica Measurements of Boundary-Layer Cloudiness and the ECMWF Diagnostic Cloud Parameterization Scheme during ASTEX. *J. Atmos. Sci.*, **52**, 2736-2751.

Byrne, R. N., R. C. J., Somerville, and B. Subasilar, 1996: Broken-cloud enhancement of solar radiation absorption. *J. Atmos. Sci.*, **53**, 878-886.

Campbell, JR, DL Hlavka, JD Spinhirne, DD Turner, and CJ Flynn, 1998: Operational Cloud Boundary Detection and Analysis from Micro Pulse Lidar Data. In *Proceedings of the 8th ARM Science Team Meeting*, Ed. by N. Burleigh and D. Carrothers, U.S. Department of Energy, Richland, WA, p. 119-122.

Clothiaux, E.E., T.P. Ackerman, G.C. Mace, K.P. Moran, R.T. Marchand, M.A. Miller, and B.E. Martner, 2000: Objective determination of cloud heights and radar reflectivities using a combination of remote sensors at the ARM CART sites. *J. Appl. Meteor.*, **38**, 645-665.

Dong, X., T.P. Ackerman, E.E. Clothiaux, P. Pilewskie, and Y. Han, 1997: Microphysical and radiative properties of stratiform clouds deduced from ground-based measurements, *J. Geophys. Res.*, **102**, 23,829-23,843.

Fouquart, Y., and B. Bonnel, 1980: Computation of solar heating of the Earth's atmosphere: a new parameterization. *Beitr. Phys. Atmos.*, **53**, 35-62.

Lane, D. E., K. Goris and R. C. J. Somerville, 2002: Radiative transfer through broken cloud fields: Observations and modeling. *J. Climate*, **15**, 2921-2933.

Lane-Veron, D. E. and R. C. J. Somerville, 2004: A physical description of stochastic shortwave radiative transfer theory. Submitted.

McClatchey, R. A., R. W. Fenn, J. E. A. Selby, F. E. Volz, and J. S. Garing, 1972: Optical properties of the atmosphere (third edition). Environmental research papers, no. 411, Air Force Cambridge Research Laboratories, Bedford, MA, 108 pp.

Stokes, G. M., and S. E. Schwartz, 1994: The Atmospheric Radiation Measurement (ARM) program: Programmatic background and design of the cloud and radiation testbed. *Bull. Amer. Meteor. Soc.*, **75**, 1202-1221.

Wiscombe, W. J., and J. W. Evans, 1977: Exponential-sum fitting of radiative transmission functions. *J. Comp. Phys.*, **24**, 416-444.